Pergamon

0013-7944(94)00187-1

Engineering Fracture Mechanics Vol. 50, No. 3, pp. 385–405, 1995

0013-7944/95 $9.50 + 0.00

INTERACTION BETWEEN FILLET AND CRACK IN ROUND AND FLAT TEST SPECIMENS

NAO-AKI NODA, TAKESHI YAMASAKI, KATSUNORI MATSUO and YASUSHI TAKASE
Department of Mechanical Engineering, Kyusyu Institute of Technology, Kitakyusyu 804, Japan

Abstract—In this paper, the stress concentration problem of a fillet in round and flat test specimens under tension is analyzed by the body force method. The stress field induced by a ring force acting in the radial and axial directions in an infinite body, and a point force in a semi-infinite plate are used as fundamental solutions to solve these problems. The stress concentration factors of a fillet in a stepped round bar and a stepped flat bar are systematically calculated under various geometrical conditions. Through comparison of the present results with previous research, it is found that Peterson's stress concentration charts based on photoelastic tests give underestimated stress concentration factors by about 13% for the worst cases. The stress distribution at the narrow section of the test specimen without a crack is investigated and the stress intensity factor of the test specimen with a fillet and a crack is systematically calculated. As a result, the geometrical condition that the interaction between the fillet and crack disappears is discussed.

1. INTRODUCTION

THE STRESS concentration analysis around a fillet is one of the most important problems in the design of high performance structures where both light weight and high strength are desirable. In addition, round and flat test specimens with fillets as shown in Fig. 1, have been used in order to investigate the mechanical properties of materials. According to Saint–Venant's principle, it seems that a fillet has a negligible effect on the stresses at distances which have the same dimensions of the diameter or the width of the narrow section of the specimen. However, taking as an example of a fatigue experiment, the analysis of the stress distribution at the narrow section and the analysis of the interaction effect among cracks and fillets are required for studying the fatigue mechanism in detail.There are few studies on the stress concentration of fillets [1–7] and the stress concentration charts in Peterson's handbook [8] have been widely used in design and research: however, there has been little discussion about their accuracy.

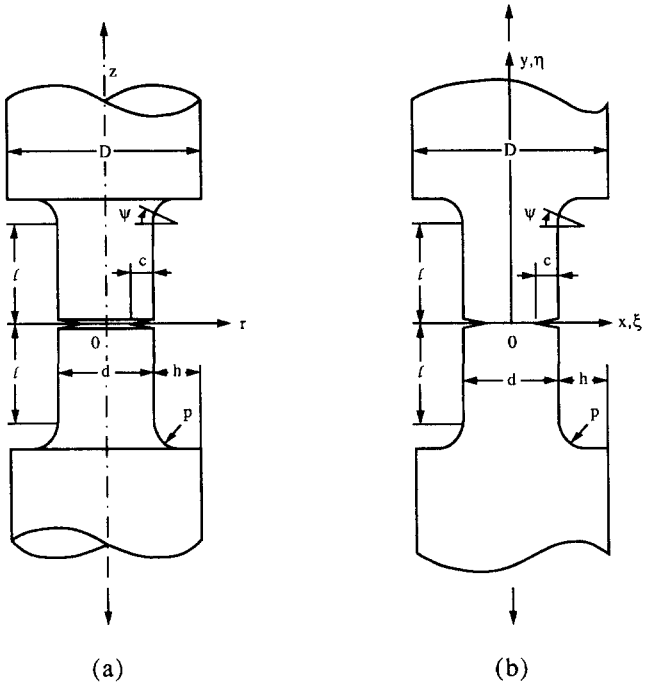

Fig. 1. Round and flat test specimens with fillet and crack.

In this paper, the problems of stress concentration in a stepped round and flat bar with a fillet under tension are analyzed using the body force method and the results are compared with previous research. In addition, the interaction effect among cracks and fillets in the round and the flat test specimens under tension, as shown in Fig. 1, is also analyzed using the body force method. First, the stress distribution at the narrow section of the test specimen without a crack [$c = 0$ in Fig. 1] is investigated; and next, the stress intensity factor of the test specimen with crack is analyzed. The fundamental solution the stress field induced by a ring force acting in the radial and axial directions in an infinite body [9, 10] is used for the analysis of round test specimens; a point force in a semi-infinite plate [11, 12] is used for the analysis of flat test specimens.

2. METHOD OF ANALYSIS

In the body force method, the stress field induced by a point force and a force doublet (a pair of point forces) in an infinite body have been used as fundamental solutions to solve problems [13]. The solution is obtained by superimposing the fundamental solutions in order to satisfy the given boundary conditions. Figure 2 shows imaginary boundaries where body forces are distributed in the analysis of a round test specimen. The body force implies a continuously embedded point force. The given boundary conditions are satisfied by applying the body force and the body force doublet along the prospective sites of stress-free boundaries for the edge and crack, respectively. In this analysis, the body force doublet is symmetrically distributed along the section FA, F′A′, E′A′, in addition to the section EA which should become a circumferential crack in order to make the shear stress τ_{rz} at the boundary $r = d/2$ small in advance. Similarly, the body forces are distributed along the boundaries BAB′ and BA′B′ in order to make the shear stress at the boundary $r = D/2$ small in advance. The method of analysis is reduced to determine the density of body force and body force doublets to satisfy the boundary conditions. In this analysis the boundaries are divided into small intervals; then, unknown functions of the body force densities are approximated by the fundamental density and stepped functions. The influence coefficients, stresses induced at the midpoint of the ith interval due to the unit distribution of body force at the jth interval are written as follows [9, 10]. Here, (ρ, ψ, ζ) is a cylindrical coordinate (r, θ, Z) where a ring force acts, and ds is the infinitesimal arc length where body forces are distributed $[ds = \sqrt{(d\rho)^2 + (d\zeta)^2}]$.

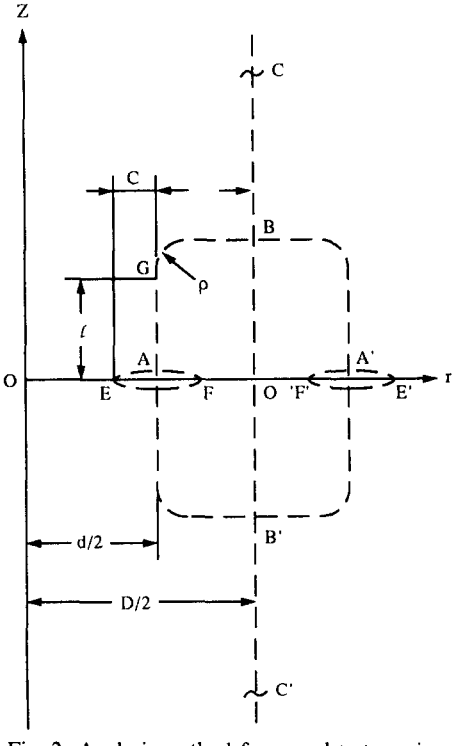

Fig. 2. Analysis method for round test specimens.

$$\left.\begin{aligned}
\sigma_i^{\rho_{DB}j} &= \int_j \sigma^{F_{DB}^*}|_{F_{DB}=1}\frac{(1-\nu)^2}{1-2\nu}\,4\sqrt{c^2-(\rho-d/2)^2}\,\mathrm{d}\rho \quad (j\text{: on crack})\\
\sigma_i^{\rho_r j} &= \int_j \sigma^{F_r^*}|_{F_r=1}\,\mathrm{d}\zeta\\
\sigma_i^{\rho_r j} &= \int_j \sigma^{F_r^*}|_{F_r=1}\,\mathrm{d}\zeta
\end{aligned}\right\}(j\text{: on surface } r=d/2 \text{ or } r=D/2)$$

$$\left.\begin{aligned}
\sigma_i^{\rho_r j} &= \int_j \sigma^{F_r^*}|_{F_r=1}\,\mathrm{d}s\\
\sigma_i^{\rho_z j} &= \int_j \sigma^{F_z^*}|_{F_z=1}\,\mathrm{d}s
\end{aligned}\right\},\quad (j\text{: on fillet}) \tag{1}$$

where $\int_j$ stands for integration of the jth interval. The integration in eq. (1) is performed numerically using Gauss' formula. When $i=j$, eq. (1) becomes singular; then, the numerical integrals are applied for the two end parts excluding $2\epsilon_0$ from the mid-part of the jth interval. For the mid-part $2\epsilon_0$, integration is carried out directly. As an example, the direct integration for crack part is expressed as follows

$$\begin{aligned}
\Delta\sigma_z^{\rho_{DB}} &= \oint_{-\epsilon_0+r_i}^{+\epsilon_0+r_i}\sigma^{F_{DB}^{**}}|_{F_{DB}=1}\frac{(1-\nu)^2}{1-2\nu}\,4\sqrt{c^2-(\rho-d/2)^2}\,\mathrm{d}\rho\\
&=\frac{1}{\pi}\sqrt{c^2-(d/2-r_i)^2}\left\{-\frac{2}{\epsilon_0}+\left[\frac{1}{r_i}\frac{d/2-r_i}{c^2-(d/2-r_i)^2}-\frac{c^2}{\{c^2-(d/2-r_i)^2\}^2}\right.\right.\\
&\quad\left.\left.-\frac{3}{8r_i^2}+\frac{1}{4r_i^2}\ln\left(\frac{8r_i}{\epsilon_0}\right)\right]\epsilon_0\right\}
\end{aligned} \tag{2}$$

where $\oint$ is interpreted in the Hadamard sense by retaining the finite part of the divergent integral and r_i is the r-coordinate of the midpoint of the ith interval. The notation $\sigma^{F_{DB}^*}$ is the stress due to a ring force doublet [9] and the notations $\sigma^{F_r^*}$, $\sigma^{F_z^*}$ are the stresses due to a ring force acting in r- and z-directions [10] in which:

$$\left.\begin{aligned}
\sigma_r^{F_{DB}^*} &= \frac{F_{DB}\rho(1-2\nu)}{4\pi(1-\nu)^2r_m^3}\left[2(1-\nu)I_0+\frac{3(1-2\nu)}{r_m^2}\rho^2(-J_0+J_2)+\frac{15\bar{z}^2}{r_m^4}(-r^2L_0+2r\rho L_1-\rho^2L_2)\right]\\
\sigma_r^{F_{DB}^*} &= \frac{F_{DB}\rho(1-2\nu)}{4\pi(1-\nu)^2r_m^3}\left[I_0+\frac{6\bar{z}^2}{r_m^2}J_0+\frac{15\bar{z}^4}{r_m^4}(-L_0)\right]\\
\tau_{rz}^{F_{DB}^*} &= \frac{F_{DB}\rho(1-2\nu)}{4\pi(1-\nu)^2r_m^3}\left[\frac{3\bar{z}}{r_m^2}(rJ_0-\rho J_1)+\frac{15\bar{z}^3}{r_m^4}(-rL_0+\rho L_1)\right]\\
\sigma_r^{F_r^*} &= \frac{F_r\rho}{4\pi(1-\nu)r_m^3}\left[(1-2\nu)(-\rho I_0-rI_1+2\rho I_2)\right.\\
&\quad\left.+\frac{3}{r_m^2}\{r^2\rho J_0-r(r^2+2\rho^2)J_1+\rho(2r^2+\rho^2)J_2-r\rho^2J_3\}\right]\\
\sigma_z^{F_r^*} &= \frac{F_r\rho}{4\pi(1-\nu)r_m^3}\left[(1-2\nu)(-\rho I_0+rI_1)+\frac{3\bar{z}^2}{r_m^2}(\rho J_0-rJ_1)\right]\\
\tau_{rz}^{F_r^*} &= \frac{F_r\rho}{4\pi(1-\nu)r_m^3}\left[(1-2\nu)\bar{z}(-I_1)+\frac{3\bar{z}}{r_m^2}\{r\rho J_0-(r^2+\rho^2)J_1+r\rho J_2\}\right]\\
\sigma_r^{F_z^*} &= \frac{F_z\rho}{4\pi(1-\nu)r_m^3}\left[(1-2\nu)\bar{z}I_0+\frac{3\bar{z}}{r_m^2}(-r^2J_0+2r\rho J_1-\rho^2J_2)\right]\\
\sigma_z^{F_z^*} &= \frac{F_z\rho}{4\pi(1-\nu)r_m^3}\left[(1-2\nu)\bar{z}(-I_0)+\frac{3\bar{z}^3}{r_m^2}(-J_0)\right]\\
\tau_{rz}^{F_z^*} &= \frac{F_z\rho}{4\pi(1-\nu)r_m^3}\left[(1-2\nu)(-rI_0+\rho I_1)+\frac{3\bar{z}^2}{r_m^2}(-rJ_0+\rho J_1)\right]
\end{aligned}\right\}, \tag{3a}$$

where

$$r_m = \sqrt{2r\rho}, \quad \bar{z} = z - \zeta,$$

$$I_n = \int_0^\pi \frac{\cos^n \phi}{(e - \cos\phi)^{3/2}}\,\mathrm{d}\phi, \quad J_n = \int_0^\pi \frac{\cos^n \phi}{(e - \cos\phi)^{5/2}}\,\mathrm{d}\phi, \quad L_n = \int_0^\pi \frac{\cos^n \phi}{(e - \cos\phi)^{7/2}}\,\mathrm{d}\phi$$

$$I_0 = \frac{1}{e^2 - 1} K_1,$$

$$I_1 = \frac{e}{e^2 - 1} K_1 - K_2,$$

$$I_2 = \frac{2e^2 - 1}{e^2 - 1} K_1 - 2eK_2,$$

$$J_0 = \frac{4e}{3(e^2 - 1)^2} K_1 - \frac{1}{3(e^2 - 1)} K_2,$$

$$J_1 = \frac{e^2 + 3}{3(e^2 - 1)^2} K_1 - \frac{e}{3(e^2 - 1)} K_2,$$

$$J_2 = -\frac{2e(e^2 - 3)}{3(e^2 - 1)^2} K_1 + \frac{2e^2 - 3}{3(e^2 - 1)} K_2,$$

$$J_3 = \frac{-8e^4 + 15e^2 - 3}{3(e^2 - 1)^2} K_1 + \frac{e(8e^2 - 9)}{3(e^2 - 1)} K_2,$$

$$L_0 = \frac{23e^2 + 9}{15(e^2 - 1)^3} K_1 - \frac{8e}{15(e^2 - 1)^2} K_2,$$

$$L_1 = \frac{e(3e^2 + 29)}{15(e^2 - 1)^3} K_1 - \frac{3e^2 + 5}{15(e^2 - 1)^2} K_2,$$

$$L_2 = \frac{-2e^4 + 19e^2 + 15}{15(e^2 - 1)^3} K_1 + \frac{2e(e^2 - 5)}{15(e^2 - 1)^2} K_2,$$

$$K_1 = \int_0^\pi (e - \cos\phi)^{1/2}\,\mathrm{d}\phi = \frac{2\sqrt{2}}{k} E(k)$$

$$K_2 = \int_0^\pi (e - \cos\phi)^{-1/2}\,\mathrm{d}\phi = \sqrt{2}kK(k). \qquad (3b)$$

The complete elliptic integrals

$$K(k) = \int_0^{\pi/2} \frac{\mathrm{d}\lambda}{\sqrt{1 - k^2 \sin^2 \lambda}}, \quad E(k) = \int_0^{\pi/2} \sqrt{1 - k^2 \sin^2 \lambda}\,\mathrm{d}\lambda$$

have the argument

$$k = \sqrt{\frac{2}{e + 1}}, \quad e = 1 + \frac{(r - e)^2 + (z - \zeta)^2}{2r\rho}.$$

The boundary conditions at the midpoint of the ith interval are expressed by using the influence coefficients as follows.

$$\sum_{j=1}^{n_1} \rho_{DB_j}\sigma_z^{\rho DB_j} + \sum_{j=n_1+1}^{n_1+n_2} (\rho_{rj}\sigma_z^{\rho_r j} + \rho_{zj}\sigma_z^{\rho_z j}) + \sigma_z^{\infty} = 0 \quad (i\text{: on crack})$$

$$\left.\begin{aligned} &\sum_{j=1}^{n_1} \rho_{DB_j}\sigma_r^{\rho DB_j} + \sum_{j=n_1+1}^{n_1+n_2} (\rho_{rj}\sigma_r^{\rho_r j} + \rho_{zj}\sigma_r^{\rho_z j}) = 0 \\ &\sum_{j=1}^{n_1} \rho_{DB_j}\tau_{rz}^{\rho DB_j} + \sum_{j=n_1+1}^{n_1+n_2} (\rho_{rj}\tau_{rz}^{\rho_r j} + \rho_{zj}\tau_{rz}^{\rho_z j}) = 0 \end{aligned}\right\} \quad (i\text{: on surface } r = d/2 \text{ or } r = d/2)$$

$$\left.\begin{aligned} &\sum_{j=1}^{n_1} \rho_{DB_j}\sigma_n^{\rho DB_j} + \sum_{j=1}^{n_1+n_2} (\rho_{rj}\sigma_{n_i}^{\rho_r j} + \rho_{zj}\sigma_{n_i}^{\rho_z j}) + \sigma_z^{\infty}\cos^2\psi_i = 0 \\ &\sum_{j=1}^{n_1} \rho_{DB_j}\tau_{nt}^{\rho DB_j} + \sum_{j=1}^{n_1+n_2} (\rho_{rj}\tau_{nt}^{\rho_r j} + \rho_{zj}\tau_{nt}^{\rho_z j}) + \sigma_z^{\infty}\sin^2\psi_i\cos\psi_i = 0 \end{aligned}\right\} \quad (i\text{: on fillet}), \tag{4}$$

where σ_z^{∞} is the nominal stress for the cylindrical diameter D, ψ_i is the angle between the r-axis and the outerward normal at the mid-point of the ith division and n_1, n_2 are division number of crack and other section, respectively. For an example, the first equation in eq. (4) corresponds to $\sigma_z = 0$ at the crack surface. Once the body force densities are determined by solving the $(n_1 + 2n_2)$ linear simultaneous eqs (4), the stresses at an arbitrary point can be obtained by using the densities and the influence coefficient.

Figure 3 shows the analysis method for the flat test specimen under tension [Fig. 1(b)]. Consider two kinds of semi-infinite plates [Fig. 3(b) and (c)]: one is defined in the range $-D/2 < x < \infty$, the other in the range $-\infty < x < D/2$. The edges $x = \pm D/2$ correspond to the stress free edges of the wide section of the plate. The stress fields of a point force in a semi-infinite plate, a Green function, can be obtained in closed form. The boundary conditions for fillets, edge and crack in the range of $x < 0$ are satisfied by using the Green function of the semi-infinite plate shown in Fig. 3(b). On the other hand, the boundary conditions in the range of $x > 0$ are satisfied by using the Green function of the semi-infinite plate shown in Fig. 3(c). As a result, the analysis method is reduced to determining the densities of the body force distribution in the semi-infinite plates shown in Fig. 3 [11, 12]. The mathematical formation for the flat test specimen can be made

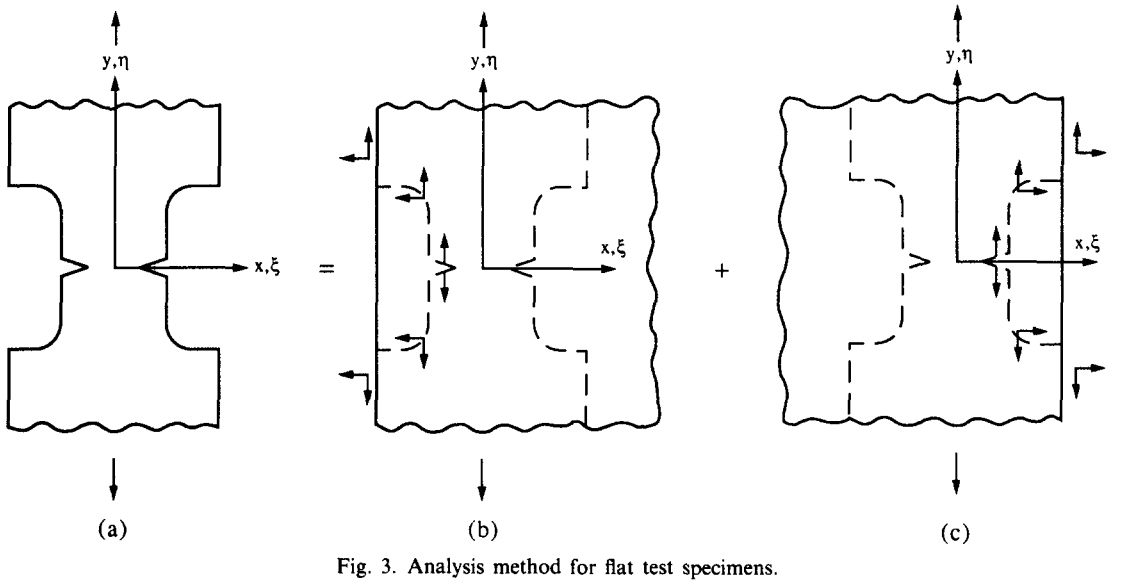

Fig. 3. Analysis method for flat test specimens.

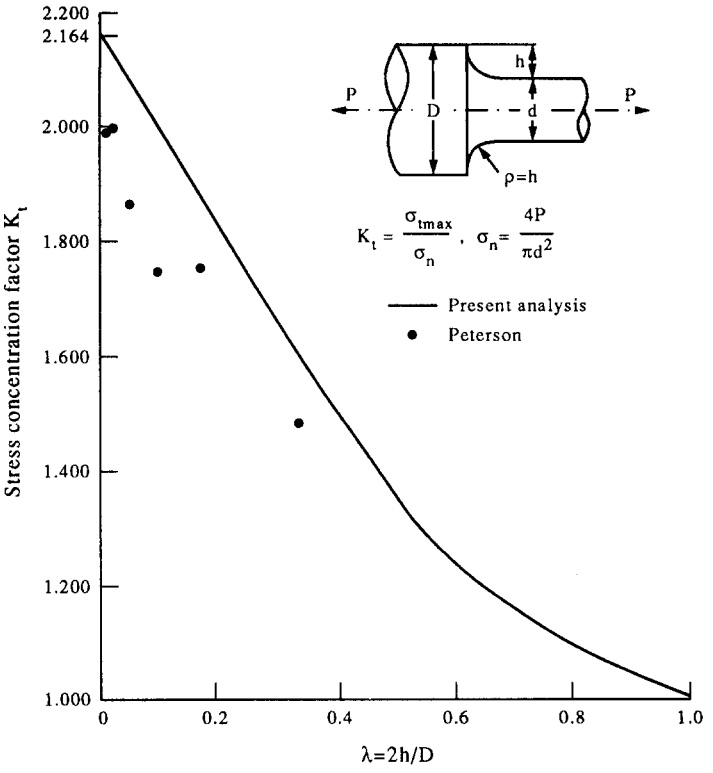

Fig. 4. SCF of stepped round bar with fillet ($\rho = h$).

in a similar manner to the round test specimen. The detail for the numerical procedure may be found in refs [13, 14].

The position of the maximum stress, which varies depending on the dimension of the fillet, cannot be known beforehand. Therefore, the fillet is divided into short intervals compared with other boundaries; the division number of the fillet is about 90 for most cases. At the midpoint of each interval, where the boundary conditions are satisfied, the normal stress in the tangential direction σ_t is also calculated; then the magnitude and the position of the maximum stresses are determined.

In the following discussion, the stress concentration factor (K_t) defined below will be used.

$$K_t = \frac{\sigma_{tmax}}{\sigma_n} \quad \sigma_n = \frac{4P}{\pi d^2} \quad \text{(round bar)}$$

$$\sigma_n = \frac{P}{d}, \quad \text{(flat bar)} \tag{5}$$

where P is the magnitude of external tensile load.

Table 1. K_t and K_t/K_{t0} of a stepped round bar with fillet

h/ρ	K_t					$K_t/K_t\|_{\lambda\to 0}$				
$\lambda = 2h/D$	0.5	1	2	4	8	0.5	1	2	4	8
0.0	1.824	2.164	2.640	3.304	4.23	1.000	1.000	1.000	1.000	1.000
0.1	1.680	1.997	2.448	3.079	3.96	0.921	0.923	0.927	0.932	0.936
0.2	1.533	1.826	2.243	2.827	3.65	0.840	0.843	0.850	0.856	0.863
0.3	1.395	1.656	2.572	2.572	3.32	0.765	0.765	0.771	0.778	0.784
0.4	1.275	1.494	1.831	2.1314	2.99	0.699	0.690	0.694	0.700	0.707
0.5	1.181	1.353	1.634	2.057	2.66	0.647	0.625	0.619	0.623	0.629
0.6	1.118	1.236	1.454	1.806	2.32	0.613	0.571	0.551	0.547	0.549
0.7	1.076	1.150	1.296	1.564	1.99	0.590	0.531	0.491	0.473	0.470
0.8	1.044	1.092	1.171	1.340	1.64	0.572	0.505	0.444	0.406	0.388
0.9	1.013	1.039	1.080	1.151	1.30	0.555	0.480	0.409	0.348	0.307
1.0	1.000	1.000	1.000	1.000	1.00	0.548	0.462	0.379	0.303	0.236

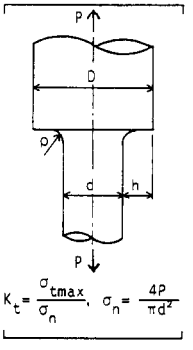

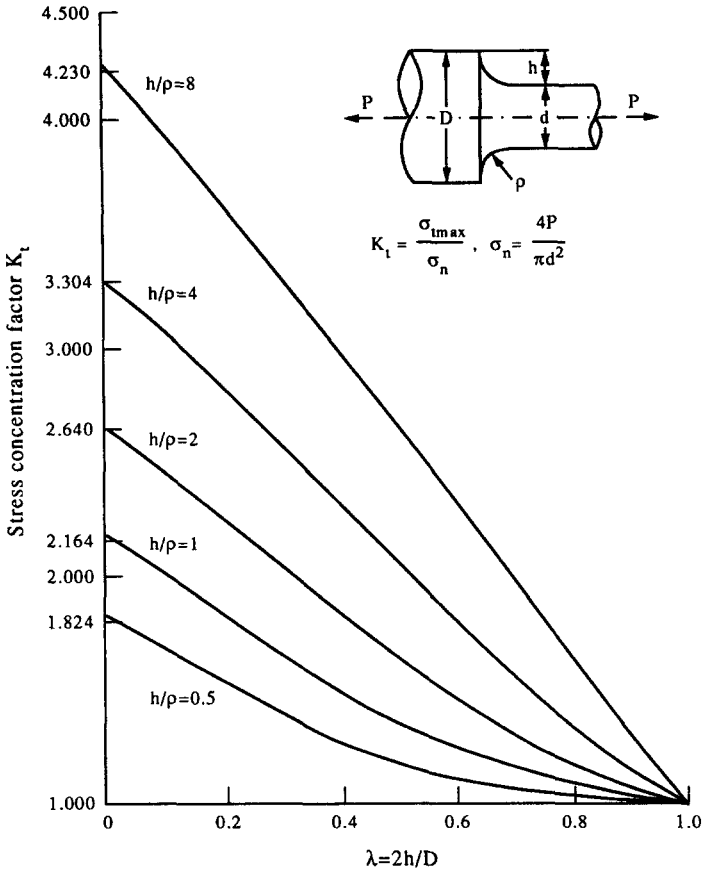

Fig. 5. SCF of stepped round bar with fillet.

The error due to the finiteness of the division number N is nearly proportional to $1/N$, the value of the stress concentration factor corresponding to $N \to \infty$ is obtained by extrapolation of the two values of K_t corresponding to the two values of N. Poisson's ratio in the case of an axisymmetric body is assumed to be 0.3.

Table 2. The position of maximum stress for stepped round bar with a fillet (degree)

h/ρ $\lambda = 2h/D$	0.5	1	2	4	8
0.0	10	13	15	18	22
0.1	10	13	15	18	22
0.2	10	13	15	18	22
0.3	9	13	15	18	22
0.4	8	12	15	18	22
0.5	6	10	13	18	21
0.6	4	8	11	16	19
0.7	3	5	9	13	17
0.8	2	3	5	9	14
0.9	0	2	3	5	8
1.0	0	0	0	0	0

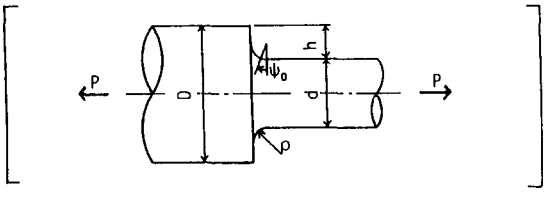

Table 3. K_t and K_t/K_{t0} of a stepped flat bar with fillet

h/ρ	K_t					$K_t/K_t\|_{\lambda\to 0}$				
$\lambda = 2h/D$	0.5	1	2	4	8	0.5	1	2	4	8
0.0	1.824	2.164	2.640	3.304	4.23	1.000	1.000	1.000	1.000	1.000
0.1	1.727	2.050	2.504	3.136	4.01	0.947	0.947	0.948	0.949	0.948
0.2	1.621	1.927	2.356	2.953	3.78	0.889	0.890	0.892	0.893	0.894
0.3	1.510	1.796	2.197	2.756	3.53	0.828	0.830	0.832	0.834	0.835
0.4	1.396	1.657	2.028	2.546	3.26	0.765	0.766	0.768	0.770	0.771
0.5	1.286	1.514	1.849	2.231	2.97	0.705	0.700	0.700	0.702	0.702
0.6	1.188	1.371	1.661	2.079	2.67	0.651	0.634	0.629	0.629	0.631
0.7	1.116	1.237	1.465	1.818	2.32	0.612	0.572	0.555	0.550	0.548
0.8	1.070	1.134	1.281	1.532	1.93	0.587	0.524	0.484	0.464	0.456
0.9	1.028	1.061	1.110	1.238	1.47	0.564	0.490	0.420	0.375	0.348
1.0	1.000	1.000	1.000	1.000	1.00	0.548	0.462	0.379	0.303	0.236

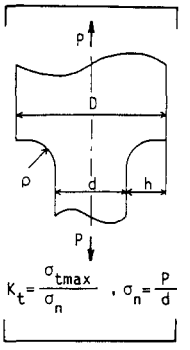

3. RESULTS AND DISCUSSION

3.1. *Case of stepped round bar with fillets under tension* [$\ell \to \infty$, c = 0 *in Fig.* 1(*a*)]

Figure 4 shows the stress concentration factor (SCF) of a stepped round bar when $\rho = h$ with varying $\lambda = 2h/D$ under tension. In Fig. 4, the value from Peterson's handbook [8] is plotted for comparison with the present analysis. Through this comparison, it is found that the result of Peterson has about 13% error for the worst cases.

Table 1 shows the SCFs of a stepped round bar with various h/ρ values under tension. The results of Table 1 are plotted in Fig. 5, where the ordinate represents the value of SCF, and the abscissa represents the relative step height $\lambda = 2h/D$. It is found that as $\lambda \to 0$, the SCF approaches the value of the stepped semi-infinite plate K_{t0}. On the other hand, as $\lambda \to 1$, the SCF approaches the value of $K_t = 1$. The position of the maximum normal stress produced at the fillet ψ_0 is shown in Table 2. In comparison with the results of stepped flat bar shown in Tables 3 and 4, it is found that when $2h/D < 0.2$ the angles ψ_0 coincide with each other. On the other hand, when $2h/D > 0.3$ the angle ψ_0 of a round bar is less than that of a flat bar.

In Fig. 6, the relation between the ratio of SCFs K_t/K_{t0} and $\lambda = 2h/D$ is shown. The ratio K_t/K_{t0} is found to be almost determined within 3% for the worst cases when $h/\rho \geqq 0.5$ and $2h/D \leqq 0.4$. Figure 7 shows the stress distribution at the narrow section of the stepped round bar when $\lambda = 0.5$ and $h/\rho = 4.2$ and 1. In Fig. 7, the stress σ_z is almost constant with a variation of 1%, at a distance of $d/2$ from the fillet when $h/\rho \leqq 2$.

Table 4. The position of maximum stress for a stepped flat bar with a fillet (degree)

h/ρ					
$\lambda = 2h/D$	0.5	1	2	4	8
0.0	10	13	15	18	22
0.1	10	13	15	18	22
0.2	10	13	15	18	22
0.3	10	13	15	18	22
0.4	10	13	15	18	22
0.5	9	13	15	18	22
0.6	7	11	15	18	22
0.7	5	8	13	17	22
0.8	2	5	9	15	20
0.9	1	3	5	8	15
1.0	0	0	0	0	0

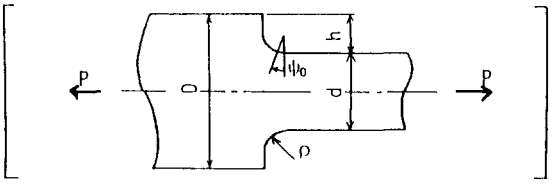

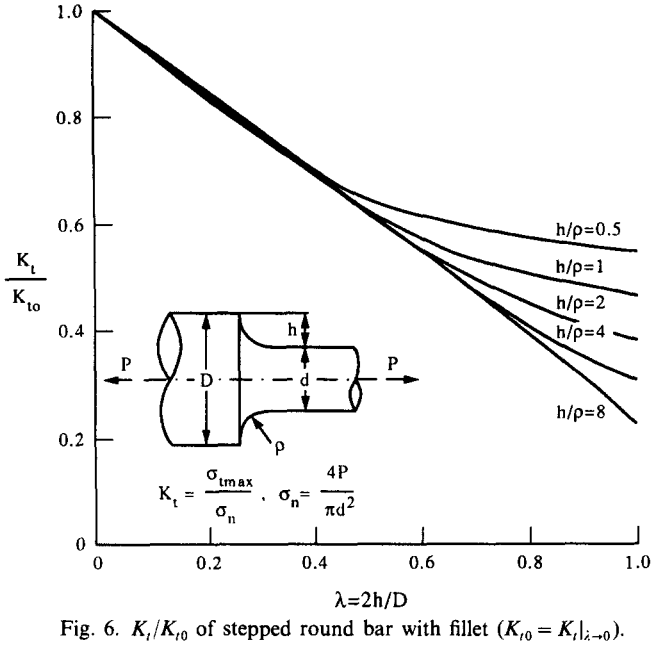

Fig. 6. K_t/K_{t0} of stepped round bar with fillet ($K_{t0} = K_t|_{\lambda \to 0}$).

3.2. *Case of stepped flat bar with fillets under tension* [$\ell \to \infty$, c = 0 *in Fig.* 1(*b*)]

Figure 8 shows the SCF of a stepped flat bar when $\rho = h$ under tension. In Fig. 8, the results of Frocht's photoelastic test [1] and the value from Peterson's handbook [8] are plotted from comparison with the present analysis. Through this comparison, it is found that the results of both Frocht and Peterson have about 10% error for the worst cases.

Table 3 shows the SCF of a stepped flat bar with various h/ρ under tension. The results of Table 3 are plotted in Fig. 9 where the ordinate represents the SCF values, and the abscissa represents $\lambda = 2h/D$. The positions of the maximum normal stresses that are produced at the fillet are shown in Table 4.

In Fig. 10, the relations between the K_t/K_{t0} ratios are found to be almost determined when $h/\rho \geqq 0.5$ and $2h/D \leqq 0.5$. Utilizing this fact, we can estimate the SCF of a stepped flat bar by using the SCF of a stepped semi-infinite plate.

Figure 11 shows the stress distribution at the narrow section of the stepped flat bar when $\lambda = 0.5$ and $h/\rho = 4.2$ and 1. In Fig. 11, the stress σ_y is almost constant with a variation of 1% at a distance of $d/2$ from the fillet when $h/\rho \leqq 2$.

3.3. *Case of round test specimen with fillets under tension* [c = 0 *in Fig.* 1(*a*)]

In Table 5, the SCF values of round test specimens with fillets under tension are shown. The SCFs when the length $\ell = 4\rho$ are shown for comparison with the SCFs when $\ell = \infty$. Through this comparison, it is found that the SCF of a round test specimen when $\ell \geqq 4\rho$ can be estimated by the SCF of a stepped round bar ($\ell = \infty$), except for the case when $h/\rho \geqq 2$ or $2h/D \leqq 0.1$.

Figure 12 shows the stress distribution at the narrow section of round test specimen for $\ell/d = 0.25$, 0.5 and 1 when $\lambda = 0.5$ and $h/\rho = 4$. In comparison with Fig. 10, a longer distance is needed to obtain a uniform stress distribution when ℓ is finite. This is probably because the two fillets located symmetrically for r-axis affect the stress distribution at the narrow section. It is found that the variation of stress distribution at the center of the test specimen is less than 1% when $\ell/d \geqq 1$.

3.4. *Case of flat test specimen with fillets under tension* [c = 0 *in Fig.* 1(*b*)]

In Table 6, the SCFs of rectangular notches with fillets in a flat bar under tension are shown. The SCFs when the length $\ell = 4\rho$ are shown for comparison with the SCFs when $\ell = \infty$. As $2h/D \to 0$, the SCF increases and approaches the value of the rectangular notch in the semi-infinite plate. Through this comparison, it is found that the SCF of rectangular notches when $\ell \geqq 4\rho$ can

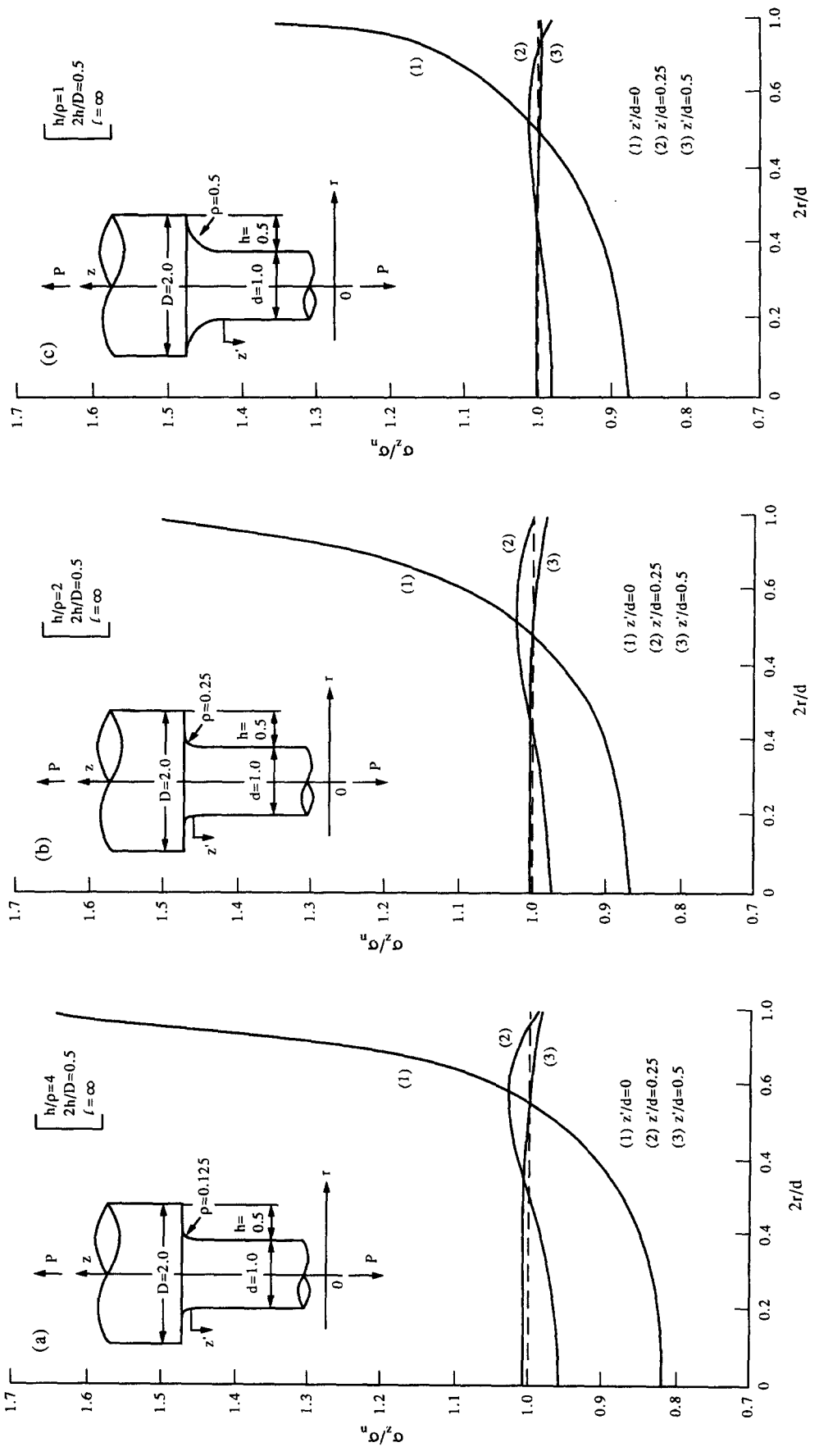

Fig. 7. Stress distribution of stepped round bar with fillet.

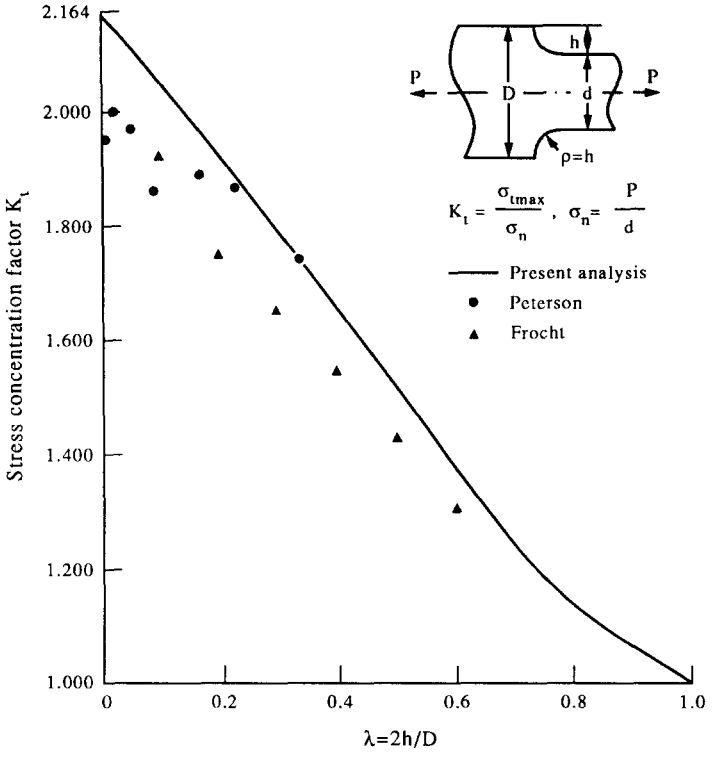

Fig. 8. SCF of stepped flat bar with fillet ($\rho = h$).

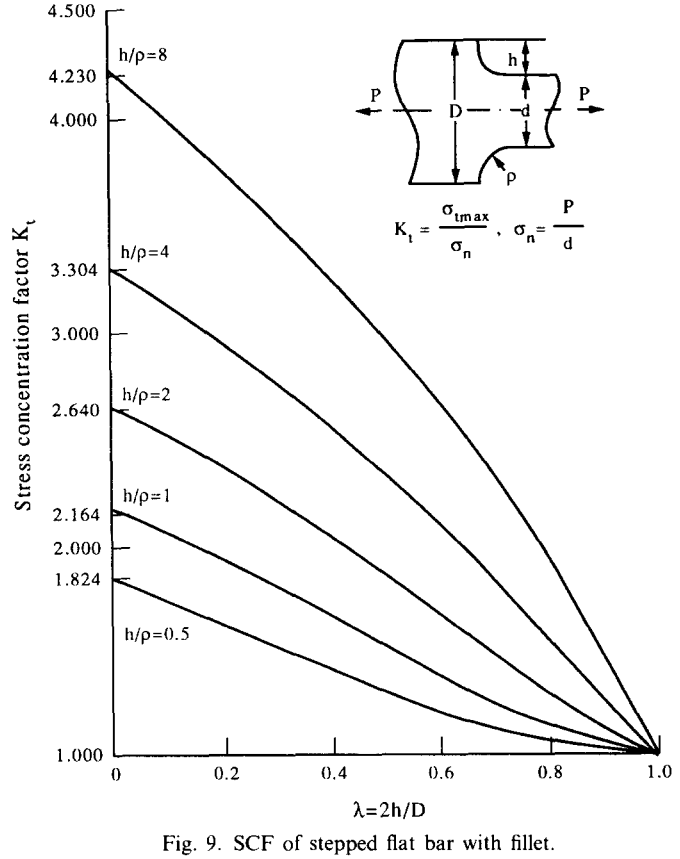

Fig. 9. SCF of stepped flat bar with fillet.

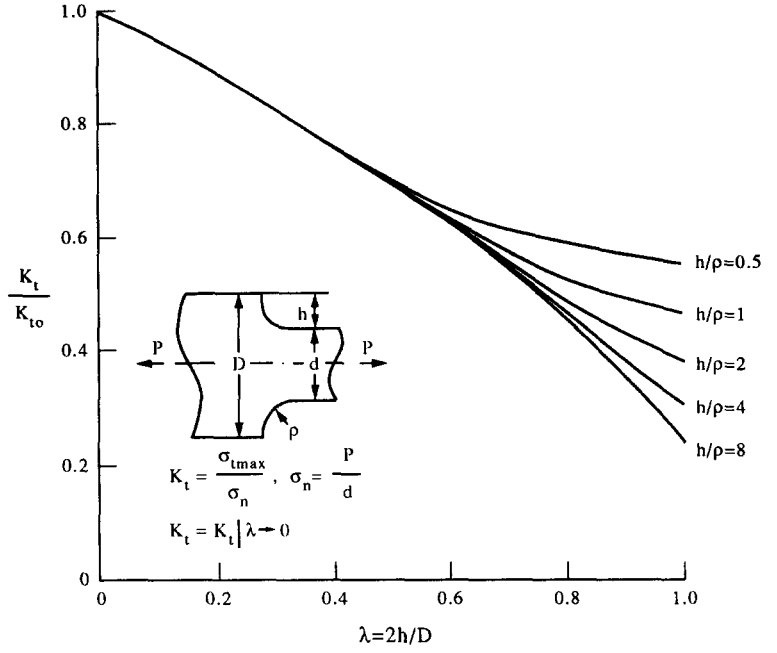

Fig. 10. K_t/K_{t0} of stepped flat bar with fillet ($K_{t0} = K_t|_{\lambda \to 0}$).

be estimated by the SCF of a stepped flat bar ($\ell = \infty$), except for the case when $h/\rho \geqq 2$ or $2h/D \leqq 0.1$.

Figure 13 shows the stress distribution at the narrow section of a flat test specimen for $\ell/d = 0.25$, 0.5 and 1 when $\lambda = 0.5$ and $h/\rho = 4$. In comparison with Fig. 11, a longer distance is needed to obtain a uniform stress distribution when ℓ is finite. The variation of stress distribution at the center of the test specimen is less than 1% when $\ell/d \geqq 1$.

3.5. *Case of round test specimen having a circumferential crack under tension [Fig. 1(a)]*

Table 7 shows the stress intensity factor F_1(SIF) of round test specimens having circumferential cracks at the center. The stress intensity factor when $\ell = \infty$ [9] and the relative error (in parentheses in Table 7) are also shown in Table 7 for comparison. The SIFs for $\ell/d = 1$ are in good agreement

Table 5. SCFs of round test specimen with fillet when $\ell = 4\rho$ (values when $\ell = \infty$ are given in parentheses)

h/ρ			
$\lambda = 2h/D$	0.5	1	2
0.0	1.879 (1.824)	2.278 (2.164)	2.869 (2.640)
0.1	1.676 (1.680)	1.990 (1.997)	2.466 (2.448)
0.2	1.531 (1.533)	1.823 (1.826)	2.227 (2.243)
0.3	1.392 (1.395)	1.654 (1.656)	2.031 (2.035)
0.4	1.272 (1.275)	1.494 (1.494)	1.830 (1.831)
0.5	1.181 (1.181)	1.353 (1.353)	1.634 (1.634)
0.6	1.118 (1.118)	1.236 (1.236)	1.454 (1.454)
0.7	1.076 (1.076)	1.150 (1.150)	1.296 (1.296)
0.8	1.044 (1.044)	1.092 (1.092)	1.171 (1.171)
0.9	1.013 (1.013)	1.039 (1.039)	1.080 (1.080)
1.0	1.000 (1.000)	1.000 (1.000)	1.000 (1.000)

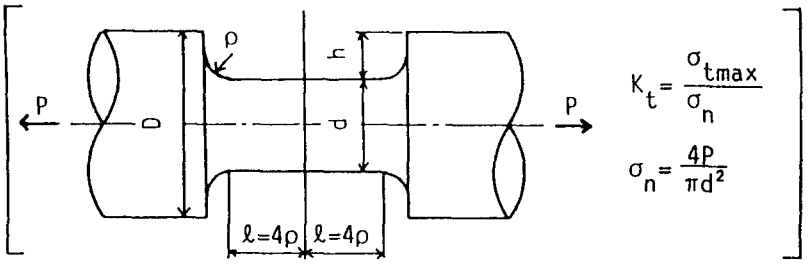

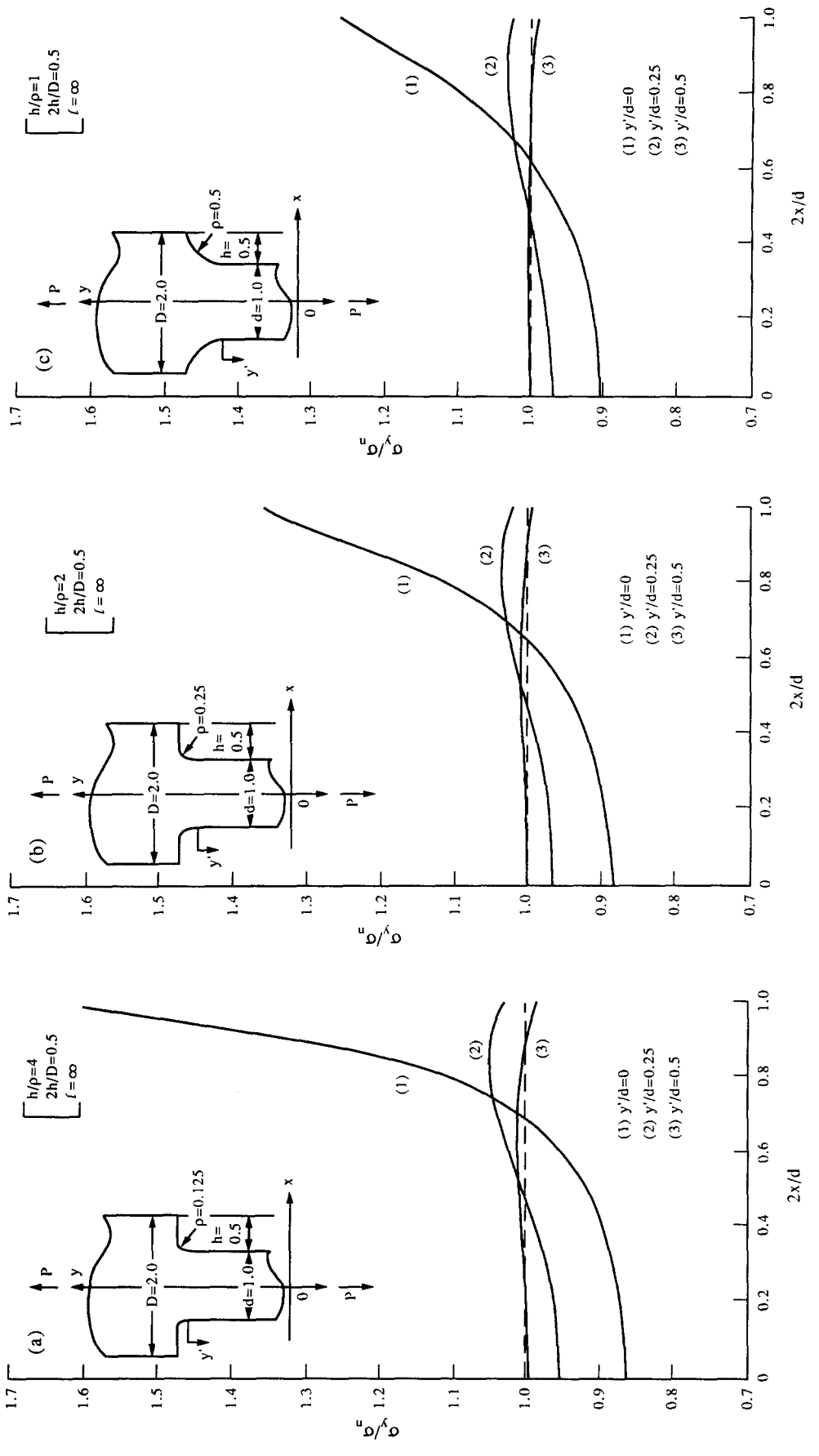

Fig. 11. Stress distribution of stepped flat bar with fillet.

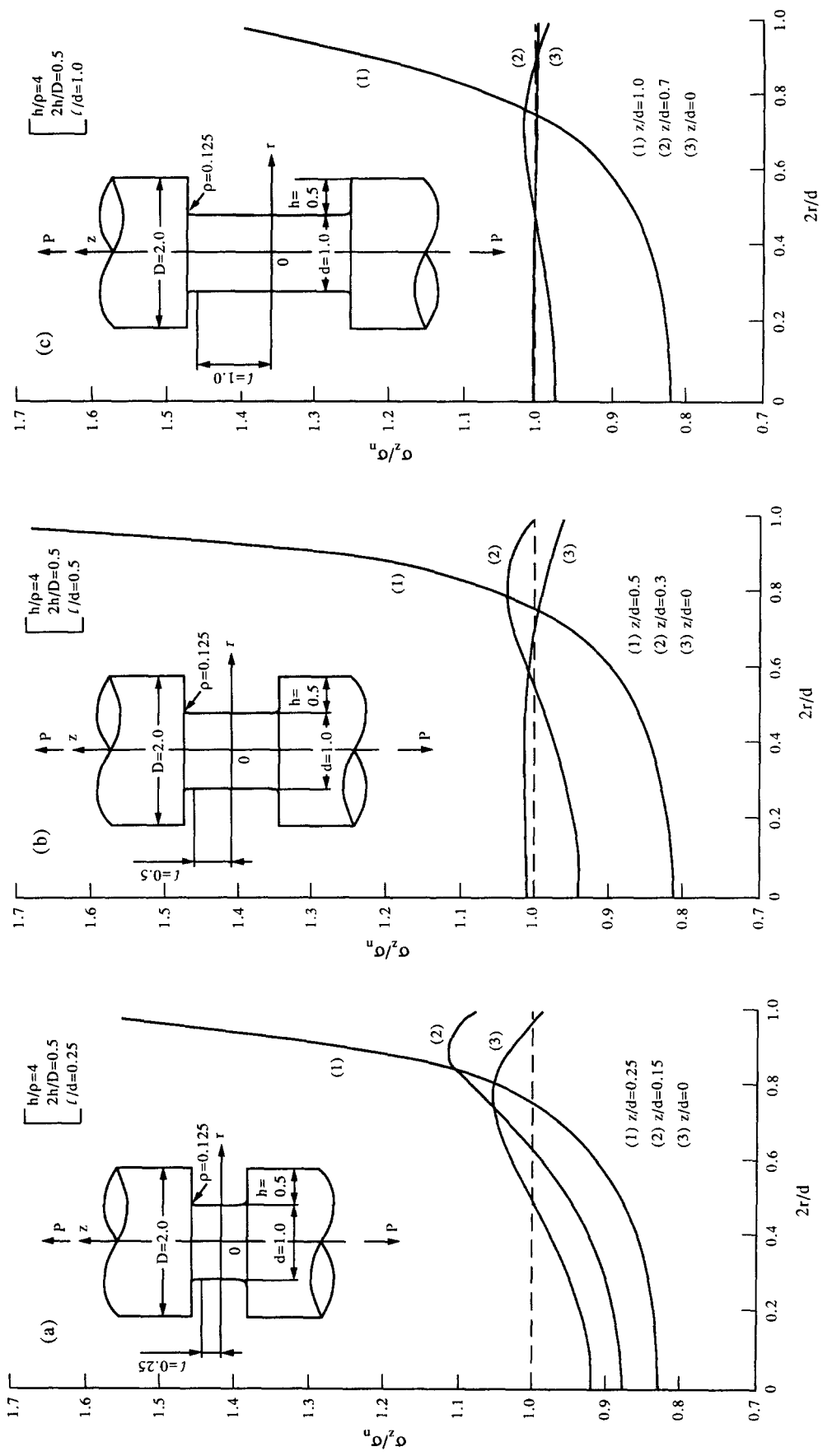

Fig. 12. Stress distribution of round test specimen with fillet.

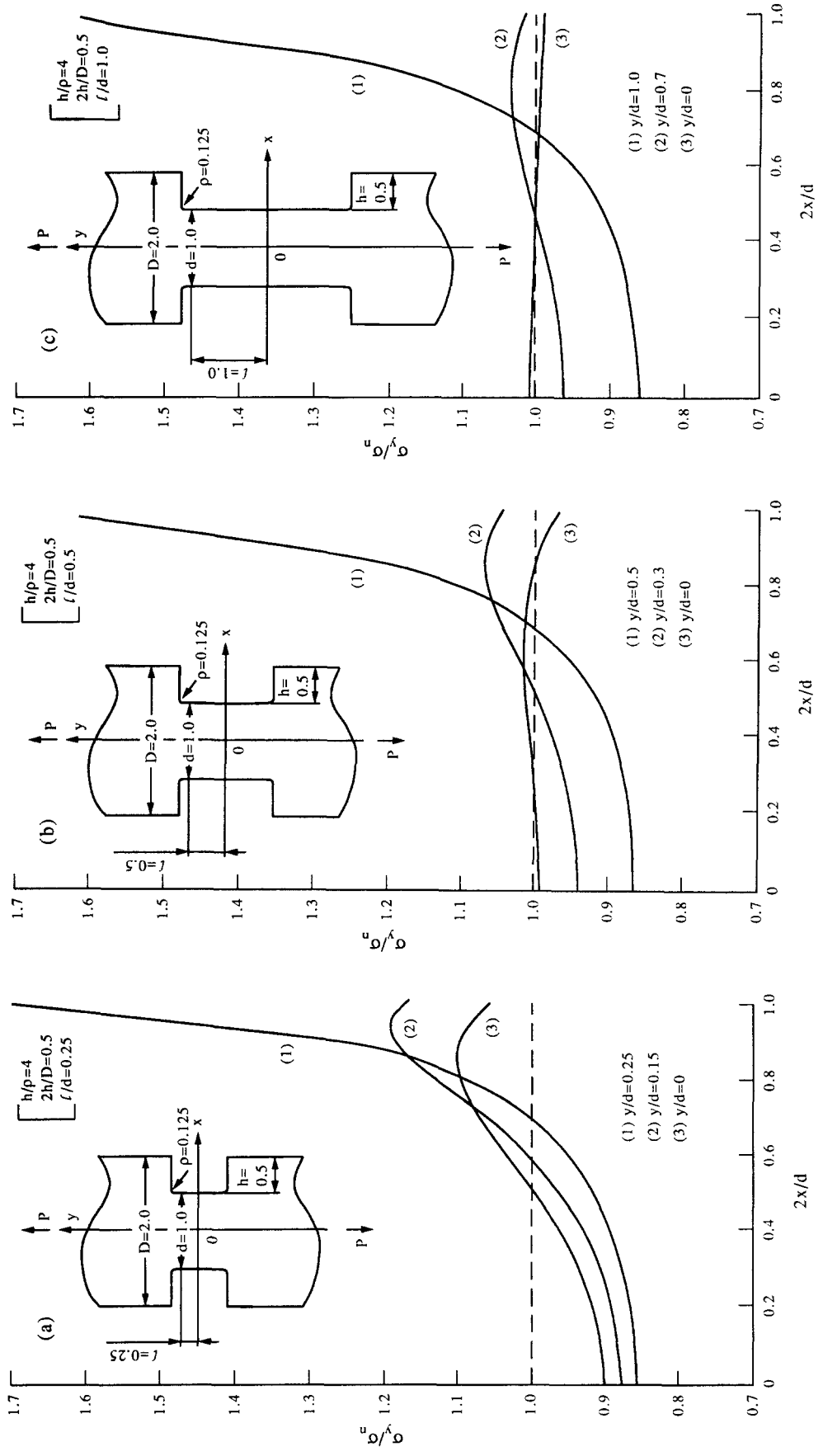

Fig. 13. Stress distribution of flat test specimen with fillet.

Table 6. SCFs of flat test specimen with fillet when $\ell = 4\rho$ (values when $\ell = \infty$ are given in parentheses)

h/ρ $\lambda = 2h/D$	0.5	1	2
0.0	1.879 (1.824)	2.278 (2.164)	2.869 (2.640)
0.1	1.724 (1.727)	2.054 (2.050)	2.571 (2.504)
0.2	1.622 (1.621)	1.923 (1.927)	2.355 (2.356)
0.3	1.511 (1.510)	1.796 (1.796)	2.188 (2.197)
0.4	1.397 (1.396)	1.658 (1.657)	2.028 (2.028)
0.5	1.287 (1.286)	1.515 (1.514)	1.850 (1.849)
0.6	1.189 (1.188)	1.371 (1.371)	1.661 (1.661)
0.7	1.117 (1.116)	1.238 (1.237)	1.465 (1.465)
0.8	1.072 (1.070)	1.134 (1.134)	1.281 (1.281)
0.9	1.029 (1.028)	1.061 (1.061)	1.110 (1.110)
1.0	1.000	1.000	1.000

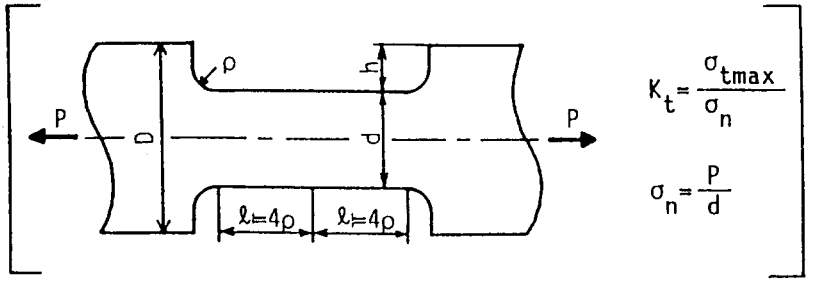

with those for $\ell = \infty$, within 0.4%. Thus, the interaction between fillet and crack may be negligible if $\ell/d \geqq 1$.

Next, we try to estimate approximately the SIFs of test specimens having a crack, as shown in Fig. 1(a), when the interaction between fillet and crack cannot be neglected. Table 8 shows SIFs of round test specimens having circumferential cracks which are calculated approximately from the distribution $\sigma_z(r)$ without a crack, as shown in Fig. 12.

$$F_I^* = \sigma_z(\lambda_c) \quad F_I|_{\ell=\infty}. \tag{6}$$

In Table 8, it is found that F_I^* is in good agreement with the results of Table 7, unless $2c/d$ is large.

3.6. *Case of flat test specimen with double cracks under tension* [*Fig.* 1(*b*)]

Table 9 shows the SIF F_I of flat test specimens with cracks at the center. The stress intensity factor of $\ell = \infty$ [15] and relative error (in parentheses in Table 9) are shown in Table 9 for comparison. The SIFs for $\ell/d = 1$ are in good agreement with the SIFs for $\ell = \infty$ within 1.0%. Thus, the interaction between the fillets and cracks may be negligible if $\ell/d \geqq 1$.

Table 10 shows the SIFs of flat test specimen with cracks which are calculated approximately from the stresses distribution without crack $\sigma_y(x)$, as shown in Fig. 13. In Table 10, it is seen that F_I^* is in good agreement with the results of Table 9, unless $2c/d$ is large.

Table 8. Estimated value of SIFs from the stress distribution without a crack (exact values are given in parentheses)

$\lambda c(=2c/d)$	0.05	0.2	0.5
$F_I\|_{\ell=\infty}$ [16]	1.150	1.261	1.940
$\ell/d =$ 0.25	1.145 (1.135)	1.299 (1.282)	1.934 (1.966)
0.5	1.113 (1.117)	1.235 (1.242)	1.963 (1.943)
1.0	1.147 (1.147)	1.257 (1.260)	1.942 (1.947)

Table 7. Dimensionless SIFs of a round test specimen with a crack [values of $(F_I - F_I|_{\ell=\infty})/F_I|_{\ell=\infty}$ 100% are given in parentheses]

λc	$(=2c/d)$		0.05				0.2				0.5	
$F_I\|_{\ell=\infty}$			1.150				1.261				1.940	
			h/ρ				h/ρ				h/ρ	
	$2h/D$	1	2	4	$2h/D$	1	2	4	$2h/D$	1	2	4
$\ell/D =$			1.181				1.306				1.968	
	0.2		(2.7)		0.2		(3.6)		0.2		(1.4)	
0.25		1.134	1.133	1.135		1.267	1.273	1.282		1.957	1.961	1.966
	0.5	(−1.4)	(−1.5)	(−1.3)	0.5	(0.5)	(0.1)	(1.7)	0.5	(1.0)	(1.1)	(1.3)
			1.135				1.261				1.952	
	0.8		(−1.3)		0.8		(0.0)		0.8		(0.5)	
			h/ρ				h/ρ				h/ρ	
	$2h/D$	1	2	4	$2h/D$	1	2	4	$2h/D$	1	2	4
			1.136				1.257				1.949	
	0.2		(−1.2)		0.2		(−0.3)		0.2		(0.5)	
0.5		1.131	1.123	1.117		1.250	1.246	1.242		1.944	1.943	1.943
	0.5	(−1.7)	(−2.3)	(−2.9)	0.5	(−0.9)	(−1.2)	(−1.5)	0.5	(0.2)	(0.2)	(0.2)
			1.137				1.254				1.945	
	0.8		(−1.1)		0.8		(−0.6)		0.8		(0.3)	
			h/ρ				h/ρ				h/ρ	
	$2h/D$	1	2	4	$2h/D$	1	2	4	$2h/D$	1	2	4
			1.147				1.261				1.948	
	0.2		(−0.3)		0.2		(0.0)		0.2		(0.4)	
1.0		1.148	1.147	1.147		1.261	1.261	1.260		1.947	1.947	1.947
	0.5	(−0.2)	(−0.3)	(−0.3)	0.5	(0.0)	(0.0)	(−0.1)	0.5	(0.4)	(0.4)	(0.4)
			1.148				1.262				1.947	
	0.8		(−0.2)		0.8		(0.1)		0.8		(0.4)	

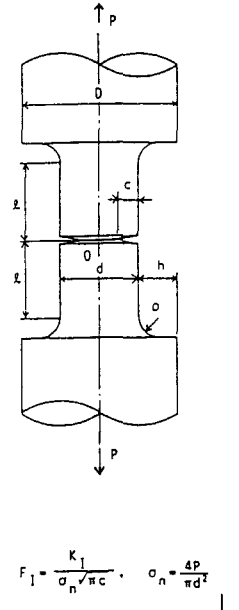

Table 9. Dimensionless SIFs of flat test specimen with a crack (values of $(F_I - F_I|_{\ell=\infty})/F_I|_{\ell=\infty}$ 100% are given in parentheses)

λc	$(=2c/d)$		0.05				0.2				0.5	
$F_I\|_{\ell=\infty}$			1.118				1.111				1.169	
			h/ρ				h/ρ				h/ρ	
	$2h/D$	1	2	4	$2h/D$	1	2	4	$2h/D$	1	2	4
$\ell/d =$			1.222				1.204				1.205	
	0.2		(9.3)		0.2		(3.0)		0.2		(3.0)	
0.25		1.147	1.172	1.195		1.154	1.180	1.202		1.195	1.207	1.216
	0.5	(2.6)	(4.8)	(6.9)	0.5	(3.8)	(6.2)	(8.2)	0.5	(2.2)	(3.2)	(4.0)
			1.114				1.121				1.179	
	0.8		(−0.4)		0.8		(0.9)		0.8		(0.8)	
			h/ρ				h/ρ				h/ρ	
	$2h/D$	1	2	4	$2h/D$	1	2	4	$2h/D$	1	2	4
			1.121				1.120				1.178	
	0.2		(0.3)		0.2		(0.8)		0.2		(0.8)	
0.5		1.094	1.091	1.090		1.099	1.099	1.100		1.168	1.169	1.171
	0.5	(−2.1)	(−2.4)	(−2.5)	0.5	(−1.1)	(−1.1)	(−1.0)	0.5	(0.1)	(0.0)	(0.2)
			1.095				1.097				1.165	
	0.8		(−2.0)		0.8		(−1.3)		0.8		−(0.4)	
			h/ρ				h/ρ				h/ρ	
	$2h/D$	1	2	4	$2h/D$	1	2	4	$2h/D$	1	2	4
			1.112				1.106				1.167	
	0.2		(−0.5)		0.2		(−0.4)		0.2		(−0.1)	
1.0		1.111	1.109	1.107		1.105	1.103	1.102		1.166	1.165	1.165
	0.5	(−0.6)	(−0.8)	(−1.0)	0.5	(−0.6)	(−0.7)	(−0.8)	0.5	(−0.3)	(−0.3)	(−0.4)
			1.114				1.107				1.167	
	0.8		(−0.4)		0.8		(0.4)		0.8		(−0.2)	

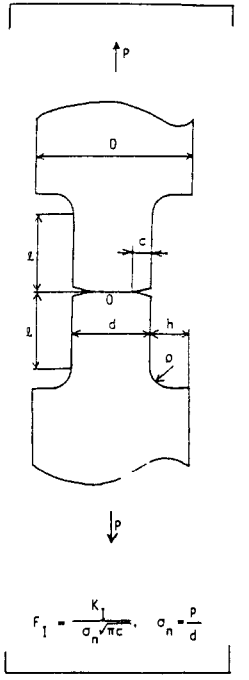

Table 10. Estimated value of SIFs from the stress distribution without crack (exact values are given in parentheses)

$\lambda c(=c/d)$	0.05	0.2	0.5
$F_1\|_{\ell=\infty}$ [9]	1.118	1.111	1.169
$\ell/d=$ 0.25	1.202 (1.195)	1.220 (1.202)	1.165 (1.216)
0.5	1.096 (1.090)	1.117 (1.110)	1.163 (1.171)
1.0	1.107 (1.107)	1.107 (1.102)	1.169 (1.165)

4. CONCLUSION

In this paper, the stress concentration problems of fillets in stepped round and flat bars under tension, and the interaction among cracks and fillets in round and flat test specimens under tension, were analyzed by the body force method. The conclusions can be summarized as follows:

(1) Through comparison of the present results for stepped round and flat bars having fillets with previous research, it was found that Peterson's stress concentration charts based on photoelastic tests give underestimated stress concentration factors by about 13% for the worst cases. The stress concentration factors were illustrated in charts (Figs 4–6 and 8–10) so they can be used easily in design or research.

(2) The SCFs of stepped flat bars with fillets were found to be almost determined by the results of shoulder fillets in a stepped semi-infinite plate (Fig. 10).

(3) The stress distributions at the narrow cross-section of stepped round and flat bars are almost constant, with a variation of 1%, at the distance $d/2$ from the fillet when $h/\rho \leqslant 2$ (Figs 7 and 11).

(4) The SCFs of test specimens, as shown in Fig. 1, were systematically calculated. It was found that the interaction between crack and fillet may be negligible when $\ell/d \geqslant 1$ (Figs 12 and 13). The SIFs can be estimated approximately from the stress distribution without crack unless the crack depth is large.

Acknowledgements—We gratefully acknowledge Prof. H. Nisitani for his helpful discussions. We would also like to thank Y. Shinmoto and K. Inoue for their assistance in programming some problems in this paper.

REFERENCES

[1] M. M. Frocht, Factors of stress concentration photoelastically determined. *J. appl. Mech.* **57,** 67–68 (1935).
[2] H. Fessler, C. C. Rogers and P. Stanley, Shouldered plate and shafts in tension and torsion. *J. Strain Anal.* **4,** 169–179 (1969).
[3] I. H. Wilson and D. J. White, Stress-concentration factors for shoulder fillet and grooves in plates. *J. Strain Anal.* **8,** 43–51 (1973).
[4] B. J. Marsden and R. H. Blakemore, Stress concentration around elliptical fillets in stepped flat bars. *J. Strain Anal.* **16,** 227–233 (1981).
[5] K. Kumagai and H. Shimada, The stress concentration factor produced by a projection under tensile load. *Bull. Jpn Soc. mech. Engrs* **11,** 739–745 (1968).
[6] M. Leven and J. B. Hartman, The stress concentration for flat bars with centrally enlarged section. *Proc. SESA* **9,** 53 (1951).
[7] A. T. Drecho and W. H. Munse, Stress concentration at external notches in members subjected to axial loading. *Univ. Illinoiss Engng Exp. Engng Sta. Bull.* No. 494 (1968).
[8] R. E. Peterson, Shoulder fillets, in *Stress Concentration Factors*, Chapter 3, pp. 80–107. John Wiley, New York (1974).
[9] H. Nisitani and N.-A. Noda, Tension of a cylindrical bar having an infinite row of circumferential cracks. *Engng Fracture Mech.* **20,** 675–686 (1984).
[10] H. Nisitani and N.-A. Noda, Stress concentration of a cylindrical bar with a V-shaped circumferential groove under torsion, tension or bending. *Engng Fracture Mech.* **20,** 743–766 (1984).
[11] N.-A. Noda and H. Nisitani, Stress concentration of a strip with a single edge notch. *Engng Fracture Mech.* **23,** 223–238 (1987).
[12] N.-A. Noda, M.-A. Tsubaki and H. Nisitani, Stress concentration of a strip with V- or U- shaped notches under transverse bending. *Engng Fracture Mech.* **31,** 119–133 (1988).
[13] H. Nisitani, The two-dimensional stress problem solved using an electric digital computer. *Jpn Soc. mech. Engrs* (JSME) **70,** 627–632 (1967). [*Bull. Jpn Soc. mech. Engrs* (JSME) **11,** 14–23 (1968)].
[14] H. Nisitani and N.-A. Noda, Stress concentration of a strip with double edge notches under tension or in-plane bending. *Engng Fracture Mech.* **23,** 1051–1065 (1986).
[15] H. Nisitani, Tension of a strip with double notches and cracks. *Trans. Jpn. Soc. mech. Engrs* (JSME) **41,** 2518–2526 (1975).
[16] D. Chen, H. Nisitani and K. Mori, Stress intensity factors of semi-infinite plate having a semi-elliptical notch with a crack under tension. *Trans. Jpn. Soc. mech. Engrs* **55,** 948–953 (1989).

(*Received* 27 *February* 1993)

APPENDIX

The stress intensity factor of a round bar with a crack emanating from a circumferential notch [Fig. A1].

This problem is important especially in relation to the research of a non-propagating fatigue crack in metals. Table A1 shows the SIFs F_I of round test specimens, with cracks and semi-circular notches, under tension. The SIFs of semi-infinite plates ($\lambda \to 0$) having a crack emanating from semi-elliptical notches [16] and the SIF of a circumferential crack without a notch ($c/h \to \infty$) in a round bar [9] are also shown in Table A1. In Table A1, it is found that $F_I/F_I|_{\lambda=0}$ is virtually determined by λ alone and almost independent of c/h. Therefore, it is found that the SIF of a round specimen [Fig. A1] can be calculated from the SIF of a semi-infinite plate, as shown in the following equation:

$$F_I|_{c/h,\lambda} = F_I|_{c/h,\lambda=0} \cdot (F_I/F_I|_{\lambda=0}). \tag{7}$$

The SIFs of cracks emanating from notches of different shapes are also calculated. As a result, it is found that the method of estimation of SIFs by eq. (7) can be applied to cracks emanating from various shaped notches.

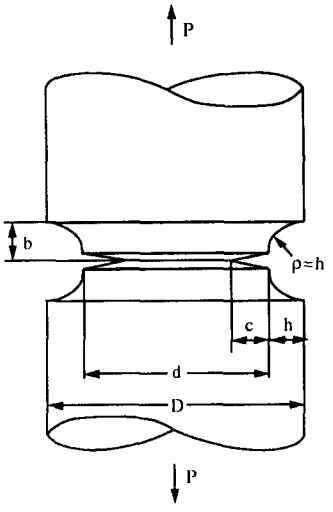

Fig. A1. A cylindrical bar having circumferential notch with a crack.

Table A1. SIFs of a cylindrical bar having a circumferential notch with a crack [example of semi-circular notch (Fig. A1) $F_I = K_I/(\sigma_n\sqrt{\pi c})$, $\sigma_n = 4P/(\pi d^2)$]

	F_I							$F_I/F_I\|_{\lambda=0}$						
c/h							∞							
$\lambda = 2(c+h)/D$	0.1	0.2	0.4	0.6	0.8	1.0	[9]	0.1	0.2	0.4	0.6	0.8	1.0	∞
0.0 [13]	0.863	1.018	1.102	1.119	1.122	1.122	1.122	1.000	1.000	1.000	1.000	1.000	1.000	1.000
0.1	0.907	1.080	1.167	1.189	1.198	1.194	1.180	1.051	1.061	1.059	1.063	1.068	1.064	1.052
0.2	0.967	1.148	1.250	1.273	1.281	1.281	1.261	1.121	1.128	1.134	1.138	1.142	1.142	1.124
0.5	1.532	1.779	1.916	1.952	1.966	1.972	1.940	1.775	1.747	1.738	1.745	1.753	1.757	1.730